Mg Metal Batteries

How to cite:
International Edition: doi.org/10.1002/anie.202301934
German Edition: doi.org/10.1002/ange.202301934

Revealing the Interfacial Chemistry of Fluoride Alkyl Magnesium Salts in Magnesium Metal Batteries

Juncai Long, Shuangshuang Tan, Junjun Wang, Fangyu Xiong, Lianmeng Cui, Qinyou An, and Liqiang Mai**

Abstract: Exploring promising electrolyte-system with high reversible Mg plating/stripping and excellent stability is essential for rechargeable magnesium batteries (RMBs). Fluoride alkyl magnesium salts ($Mg(OR^F)_2$) not only possess high solubility in ether solvents but also compatible with Mg metal anode, thus holding a vast application prospect. Herein, a series of diverse $Mg(OR^F)_2$ were synthesized, among them, perfluoro-tert-butanol magnesium ($Mg(PFTB)_2$)/$AlCl_3$/$MgCl_2$ based electrolyte demonstrates highest oxidation stability, and promotes the in situ formation of robust solid electrolyte interface. Consequently, the fabricated symmetric cell sustains a long-term cycling over 2000 h, and the asymmetric cell exhibits a stable Coulombic efficiency of 99.5 % over 3000 cycles. Furthermore, the Mg||Mo_6S_8 full cell maintains a stable cycling over 500 cycles. This work presents guidance for understanding structure–property relationships and electrolyte applications of fluoride alkyl magnesium salts.

Introduction

Rechargeable magnesium batteries (RMBs) directly using magnesium (Mg) metal as anode do not suffer from dendrite growth in most cases.[1] In addition, Mg also features low cost, high resource abundance (1.94 % in earth's crust), and low reduction potential (−2.37 V vs. standard hydrogen electrode), making RMB anticipated to be the next generation of energy storage devices.[2] However, distinguished from monovalent (Li/Na/K) metal batteries, the reduction of conventional carbonate electrolytes will generate a Mg^{2+}-insulating solid electrolyte interface (SEI) between Mg anode and electrolyte, blocking the Mg^{2+} transport and reversible plating/stripping.[3] Up to date, reversible Mg plating/stripping process can only be achieved in Mg-compatible ether electrolyte,[4] the evolution of RMBs is driven by the development of new electrolyte-system.

In 2000, Aurbach et al. constructed a prototype system for RMBs by combing Mg organohaloaluminate salts ($Mg(AlCl_3R)_2$ and $Mg(AlCl_2RR')_2$, R and R′ are alkyl groups) electrolyte with Mo_6S_8 cathode.[5] Subsequently, researchers further modified the anionic structure of the electrolyte via in situ reaction of functional magnesium salts such as PhMgCl,[6] ROMgCl (RO are different phenolic groups),[7] $MgCl_2$[8] with $AlCl_3$ to obtain the electrolyte with wider electrochemical window. Structure and functional groups of Mg salts strongly influence the properties of electrolytes.[9] Follow this direction, in recent years, fluorinated boron center Mg electrolytes such as $Mg[B(hfip)_4]_2$,[10] $Mg[B(Otfe)_4]_2$[11] have been extensively utilized due to their comprehensive properties. However, boron-based reagents always accompanied by exorbitant costs and complex synthesis processes.[12] Fluoride alkyl magnesium salts ($Mg(OR^F)_2$, R^F represents fluoride alkyl) not only versatile in structure and convenient in synthesis, but also have high solubility in ether reagents, which have a promising application potential in Mg electrolyte. Very recently, Zhang et al. have already demonstrated the potential of perfluorinated tert-butoxide magnesium salt as all-magnesium salt electrolyte, however, the oxidative stability of this electrolyte is still insufficient (3.1 V vs. Mg/Mg^{2+}).[13] The low stability of electrolytes hinders the exploration of high-voltage cathode materials, limiting the energy density of RMBs and losing competitiveness. Regulating the interfacial chemistry of $Mg(OR^F)_2$-based electrolytes, broadening the electrochemical window and accessing high-voltage electrolytes is a major challenge in this field.

Herein, we design and synthesize a family of $Mg(OR^F)_2$ for Mg electrolytes and systematically investigated the influence of the amount and position of trifluoromethyl ($-CF_3$) for the electrochemical performance of electrolytes. The results suggest that the presence of $Mg(OR^F)_2$ salts effectively modify the local coordination environment of Mg^{2+} in electrolytes and strengthened the oxidative stability of electrolytes (up to 4 V vs. Mg/Mg^{2+}). Among them, perfluoro-tert-butanol magnesium ($Mg(PFTB)_2$)/$AlCl_3$/$MgCl_2$-DME (1,2-dimethoxyethane) based electrolyte containing more $-CF_3$ group also beneficial for the in situ generation of a robust fluorinated organic–inorganic composite SEI. Based on these distinctive properties, Mg||Mg

[*] J. Long, J. Wang, Dr. F. Xiong, L. Cui, Prof. Q. An, Prof. L. Mai
State Key Laboratory of Advanced Technology for Materials Synthesis and Processing, Wuhan University of Technology
Wuhan, 430070 (China)
E-mail: anqinyou86@whut.edu.cn
mlq518@whut.edu.cn
Dr. S. Tan
College of Materials Science and Engineering, Chongqing University
Chongqing 400030 (China)
Prof. Q. An, Prof. L. Mai
Wuhan University of Technology (Xiangyang Demonstration Zone)
Xiangyang 441000 (China)

symmetric cell with this electrolyte sustains a long-term cycling over 2000 h at a current density of 0.5 mA cm^{-2} with an extremely low polarization of 50 mV. In addition, the Mg||Cu half-cell demonstrates an average Coulombic efficiency (CE) above 99.5 % over 3000 cycles. Moreover, the Mg||Mo_6S_8 full cell maintains 93 % capacity retention at 1 C after 500 cycles, which exhibiting the potential of this fluoride alkyl electrolyte.

Results and Discussion

$Mg(OR^F)_2$ were synthesized through a one-step "transmetalation reaction" between di-n-butyl magnesium ($MgBu_2$) and various fluorinated alcohols.[14] According to the amount and position of –CF_3 group, the as-synthesized $Mg(OR^F)_2$ salts were designated as $Mg(TFE)_2$ (mono-CF_3 substituted), $Mg(HFIP)_2$ (bis-CF_3 substituted), $Mg(PFTB)_2$ (tris-CF_3 substituted), respectively. To authenticate the favorable effects of fluoride alkyl substitution, magnesium methoxide ($Mg(OMe)_2$) without –CF_3 group was employed as a comparison. The mass spectrometry (MS) results and structural formulas of these Mg salts are shown in Figure S1. As fluorination of $Mg(OR^F)_2$ increases, the mass-to-charge ratio (m/z) of various Mg salts are correspondingly raised, typically, $Mg(PFTB)_2$ demonstrates the main m/z value of 495. The successful substitution of fluoride alkyl was further confirmed by spectroscopic characterization. From Fourier transform infrared (FTIR) spectra (Figure S2), the peak assigned to the vibration of the C–H bond (1447 cm^{-1}) gradually weakens and the peaks corresponded to the vibrations of –CF_3 (731 cm^{-1} and 1172 cm^{-1}) appear in $Mg(OR^F)_2$ samples.[15] In addition, the vibrations of the Mg–O bond (529 cm^{-1} and 1628 cm^{-1}) and the C–O (1093 cm^{-1}) bond can be detected in each sample.[16] In ^{19}F nuclear magnetic resonance (NMR) spectra, the three $Mg(OR^F)_2$ salts show singlet peak corresponding to –CF_3 group near −75 ppm (Figure S3a), which is consistent with previously reported result.[17] However, some discrepancies in ^{13}C NMR shifts were observed, suggesting that the substitution of –CF_3 for –H leads to chemical shift of C peak (Figure S3b).[18]

Inspired by previous research, the electrolyte activity of $Mg(OR^F)_2$ was further boosted by inorganic chlorides.[19] In brief, fluoride alkyl electrolytes were prepared by adding $Mg(OR^F)_2$, $MgCl_2$, and $AlCl_3$ to DME solvent in a certain order then stirring. The as-prepared electrolytes were separately named as MOME (with $Mg(OMe)_2$), MTFE (with $Mg(TFE)_2$), MHFP (with $Mg(HFIP)_2$), and MPFB (with $Mg(PFTB)_2$) according to the used Mg salts. Besides, a $Mg(OR^F)_2$-free electrolyte was also prepared for comparison, which is commonly known as MACC electrolyte. Eventually, MOME electrolyte is cloudy in ether reagents, but the other electrolytes are soluble and clarified (Figure S4), demonstrating the improved solubility of $Mg(OR^F)_2$ owing to the replacement of –CF_3 group. The anionic species of these clarified electrolytes were investigated by MS. In MACC electrolyte, the dominant anion structure is [$AlCl_4^-$] (m/z of 168.85), which has been already confirmed (Figure S5).[20] While in fluoride alkyl electrolytes, the anion species show distinct differences according to the degree of fluorination of $Mg(OR^F)_2$. In MTFE electrolyte, [$AlCl_4^-$] anions still dominate and the anion component of the electrolyte varies slightly (Figure 1a), which implies that $Mg(TFE)_2$ with single –CF_3 group shows a limited effect on active ions in electrolyte. Furthermore, in MHFP electrolyte, [HFIP·Cl_2^-] anions (m/z of 202.97) are most abundant (Figure 1b), suggesting the gradual dominance of fluorinated anions in the solution. When it comes to MPFB electrolyte, only the signal of [$PFTB^-$] (m/z of 234.98) can be detected, which indicates the absolute predominance of [$PFTB^-$] (Figure 1c). These results indicate that the addition of $Mg(OR^F)_2$ can affect the components of the anion in the electrolyte. Single-crystal XRD diffraction was employed to demonstrate the modified electrolyte structure. Figure S6 and Table S1–2 present the ORTEP plots and crystal structure details, respectively. It is worth noting that the crystallized MPFB electrolyte exhibited two distinct crystal structures, which suggests that the specific coordination structure in electrolyte is not well represented. Therefore, molecular dynamics (MD) simulations were performed to characterize the solvation structure of these electrolytes. Figure 1d–f reveals a significant difference between MACC electrolyte and the modified electrolyte. Specifically, the fluoride alkyl group partially replaces the Cl^- and binds directly to the Mg^{2+}, enveloping it like a shell. By combining the radial distribution functions (Figure 1g–i), we were able to quantify the local coordination environment of Mg^{2+} in various electrolytes. Furthermore, the effectiveness of this fluoride alkyl-rich solvation structure was further verified by density functional theory (DFT) calculations.[21] As shown in Figure S7, compared with [Mg−2Cl−3DME], the introduction of fluoride alkyl group into the first solvation sheath leads to decreased lowest unoccupied molecular orbital (LUMO) and highest occupied molecular orbital (HOMO) energy level. Notably, [Mg−Cl−PFTB−2DME] exhibit lowest LUMO and HOMO energy levels (0.06 eV and −8.29 eV, respectively), implying that MPFB electrolyte is more vulnerable to be reduced and more difficult to be oxidized.[22] Besides, electrostatic potential (ESP) and natural bond orbitals (NBO) maps in Figure S8 reveal the dispersion of the negatively charged zones in [$HFIP^-$] and [$PFTB^-$] groups compared to [$AlCl_4^-$], as well as the increase of dipole moment (Table S3).[23] The oxidation stability of electrolytes is also closely associated with the component most susceptible to oxidation, and in Mg electrolytes it is frequently the anions.[24] The more uniformly distributed potential suggests the possibilities of higher theoretical oxidative stability of fluoride alkyl electrolytes.[25] The presence of electron-withdrawing –CF_3 group in these electrolytes makes it difficult to lose electrons and oxidize.[26] The results from theoretical calculations confirm the effectiveness of introducing fluoride alkyl magnesium salts, as it can enhance the oxidation stability of electrolytes by reconstructing the solvation structure of Mg^{2+} in solvent.

Mg plating and stripping capability of these electrolytes was investigated in a three-electrode system employing cyclic voltammetry (CV). No reversible Mg plating/stripping

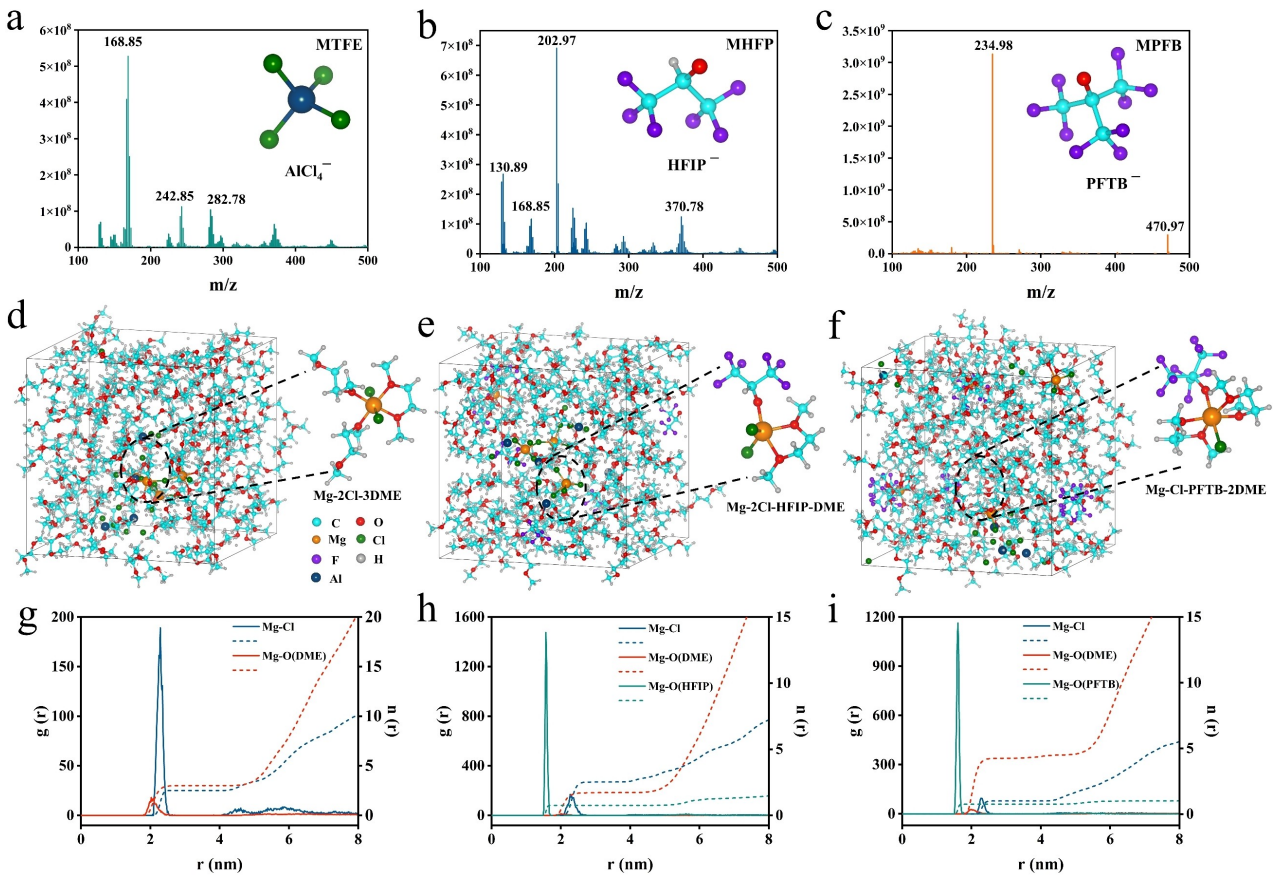

Figure 1. Experiment and theoretical studies of electrolyte solvation structures. MS results of the a) MTFE electrolyte, b) MHFP electrolyte and c) MPFB electrolyte. Molecular dynamics (MD) simulation snapshots of d) MACC electrolyte, e) MHFP electrolyte, and f) MPFB electrolyte. Radical distribution functions calculated from MD simulations of g) MACC electrolyte, h) MHFP electrolyte, and i) MPFB electrolyte.

processes were observed in MOME electrolyte (Figure S9). In contrast, all three fluoride alkyl electrolytes display reversible plating/stripping behavior (Figure 2a–c). Compared with MACC electrolyte (Figure S10), they have a single deposition peak, which implies that the irreversible deposition of aluminum is inhibited. Nevertheless, the maximum current density of MTFE and MHFP electrolytes are significantly lower, suggesting that Mg redox kinetics in these electrolytes is slower than in MPFB electrolyte.[27d] In addition, linear sweep voltammetry (LSV) was carried out to check the highest voltage tolerance of these electrolytes (Figure 2d). Unlike MACC, which tends to decompose around 3.2 V,[20] all the fluoride electrolytes exhibit a wider electrochemical window, especially the oxidation potential of MPFB electrolyte up to 4 V (vs. Mg/Mg^{2+}). This result coincides well with the DFT calculations presented above, and proves the impact of solvation structure on the electrolyte oxidation stability. Unfortunately, although simple fluoride alkyl magnesium salts have good oxidative stability in various metal substrates (Figure S11), the high oxidation stability of electrolyte is only achieved on a stable molybdenum (Mo) substrate, due to the presence of Cl^- in the electrolyte, other common metal substrates start to be corroded around 2 V (Figure S12).[28] Mg||Cu asymmetric cells were assembled to evaluate the Mg plating/stripping CE in different electrolytes at 0.5 mA cm^{-2} (Figure 2e). In cells with MACC and MTFE electrolyte, the Mg plating/stripping potentials fluctuate dramatically during the cycle and then turn totally short circuit (Figure S13a and S13b). On the contrary, cells with MHFP and MPFB electrolytes exhibit stable CEs over 3000 times. It is worth mentioning that the voltage hysteresis of MHFP increases (from 190 mV to 470 mV) during the cycle and the corresponding CE fluctuates more (Figure S13c), but the voltage hysteresis of MPFB is constantly smooth (from 100 mV to 210 mV) and the average CE reaches to 99.5 % (Figure S13d).

Mg anode stability in different electrolytes was evaluated using Mg||Mg symmetric cells. As illustrated in Figure 2f, keep the areal capacity at 0.5 mAh cm^{-2}, when the current density gradually increases to 1 mA cm^{-2}, both MACC and MTFE suffer a short circuit. In contrast, MHFP and MPFB consistently maintain a low overpotential, even at a high current density of 5 mA cm^{-2}, the voltage hysteresis of these electrolytes is only about 360 mV. Moreover, when the current density dropped back to 0.1 mA cm^{-2}, the overpotential also returned to 40 mV, demonstrating the good reversibility of MHFP and MPFB electrolytes. In addition, the long-term cyclability of these electrolytes was further evaluated at 0.5 mA cm^{-2} and 0.5 mAh cm^{-2} (Figure 2g). The voltages suddenly decrease over a period time in the case of

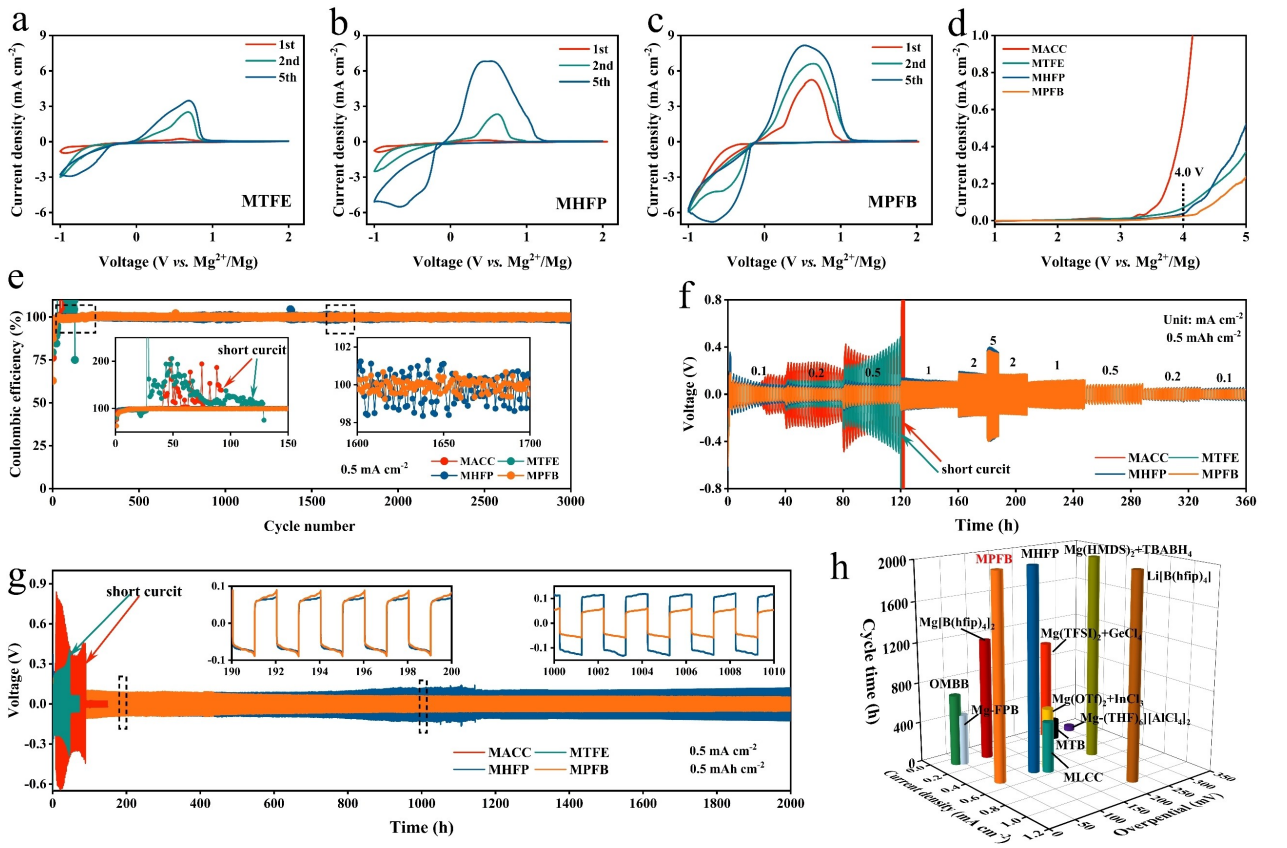

Figure 2. Electrochemical performance. Cyclic voltammograms of the Mg plating and stripping process using a) MTFE electrolyte, b) MHFP electrolyte, and (c) MPFB electrolyte. The CV was studied by a three-electrode system using Mg as the reference and counter electrode and Mo as the working electrode at a scanning rate of 25 mV s^{-1}. d) Oxidation stability of four electrolytes in Mg||Mo half cells tested by LSV. e) Mg plating/stripping CE in Mg||Cu half cells using four electrolytes at 0.5 mA cm^{-2} and 0.25 mAh cm^{-2}. Insets show an enlarged view at the cycles framed by the two dashed rectangles. f) Overpotentials of Mg||Mg symmetric cells in four electrolytes at various current densities from 0.1 to 5 mA cm^{-2} with a fixed capacity of 0.5 mAh cm^{-2}. g) Galvanostatic Mg plating/stripping in Mg||Mg symmetric cells at 0.5 mA cm^{-2} and 0.5 mAh cm^{-2}. Insets show the detailed voltage profiles of the symmetric cells in different electrolytes at the cycles framed by the two dashed rectangles. h) Performance comparison of the reported electrolytes with MHFP and MPFB electrolytes.

MACC and MTFE electrolytes, which is attributed to the occurrence of a short circuit. In contrast, steady polarization voltages were observed in cells with MHFP (≈110 mV) and MPFB (≈50 mV) electrolytes for 2000 h. Even compared with conventional Mg electrolytes, MPFB electrolyte also exhibits the lowest polarization at 0.5 mA cm^{-2} (Figure 2h, Table S4).[10a,12a,15,18,27]

Apparently, the influence of fluoride alkyl magnesium salts on electrolyte properties is well beyond oxidation stability, different electrolytes show great discrepancies in cycling stability. We speculate that differences in Mg deposition morphology also play a significant role, as shown in the scanning electron microscopy (SEM) images of the Mg anode after deposition (Figure S14), these electrolytes all exhibit dendrite-free deposition characteristics. However, MHFP and MPFB show more homogeneous deposition, which might be one of the factors to maintain a long-term stable cycle. Along this direction, we further investigated the composition of the SEI on cycled Mg anode, looking to identify the key factors determining the stability of cells.

Sacrificing a tiny portion of the electrolyte during the initial cycles to generate a stable SEI layer at the electrolyte-anode interface impacts the cell significantly.[29] The anions of fluoride alkyl electrolytes have an enhanced tendency to form SEI due to the higher degree of terminal fluorination.[30] The above-mentioned DFT calculations have confirmed the lower LUMO values in fluoride alkyl electrolytes, which makes it easier to decompose at low potentials, forming an anion-derived SEI layer. Therefore, we further investigated the evolution of SEI on cycled Mg anode through in situ electrochemical impedance spectroscopy (EIS). The results after fitting through the equivalent circuit (Figure S15) are shown in Figure 3. For pure MACC electrolyte, the charge transfer resistance (R_{ct}) of Mg||Mg symmetric cell decreases significantly after cycling (from 688 Ω to 61 Ω), which is attributed to the accumulation of Cl^- on Mg surface in the chlorine-containing electrolyte (Figure 3a).[9a] However, no new semicircle was observed in the Nyquist plot even after 20 cycles, suggesting that no SEI is formed. That may be the underlying reason for the poor cycle stability in this electrolyte. While in the MTFE

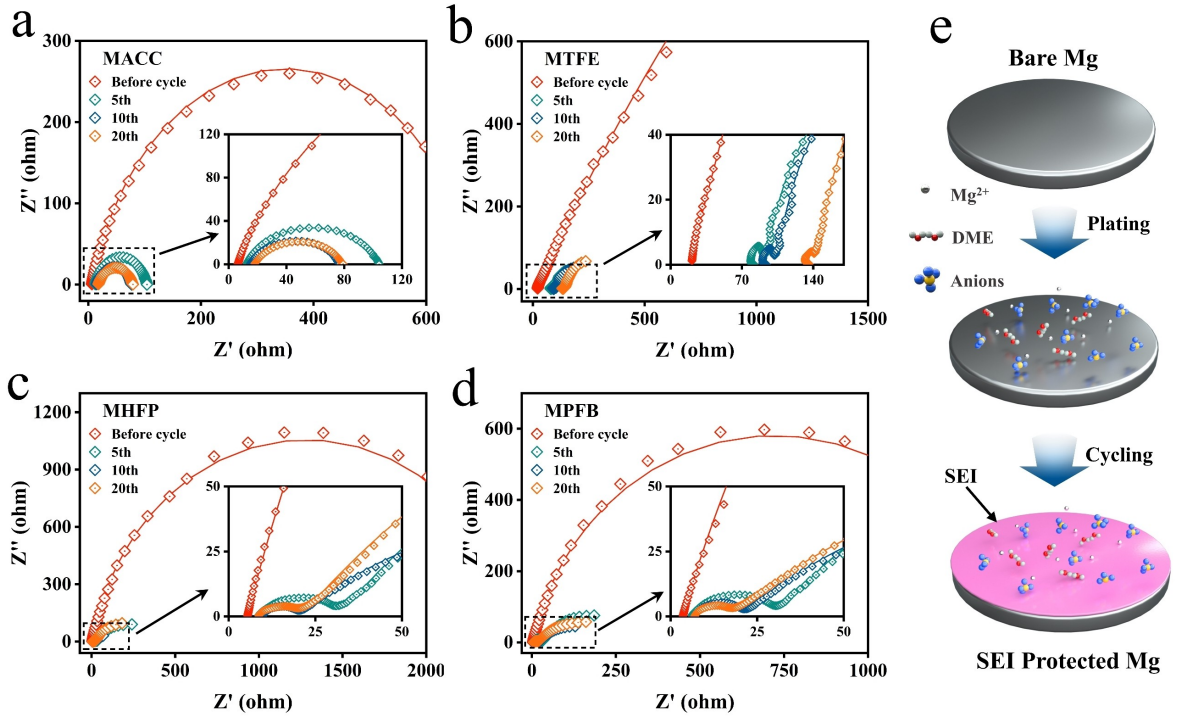

Figure 3. Characterization of the in situ generated SEI layer. In situ EIS results for the Mg||Mg symmetric cells after varied cycles in a) MACC electrolyte, b) MTFE electrolyte, c) MHFP electrolyte, and d) MPFB electrolyte. The dots in the Figure are the test results and the solid lines are the fitting result. The inset shows an enlarged view at the cycles framed by the dashed rectangles. e) Schematic diagram of the SEI layer generation process.

electrolyte, a similar process of R_{ct} decrease can also be noticed (Figure 3b). In addition, a new semicircle emerged on the Nyquist plot after 5 cycles, implying that the addition of $Mg(OR^F)_2$ indeed contributes to the formation of SEI.[31] However, the internal resistance (Rs) of the cell keeps increasing as the cycle proceeds (from 18 Ω to 132 Ω), indicating that this SEI layer is ineffective in stabilizing the Mg-electrolyte interface and hence the electrochemical performance of MTFE is unacceptable. When it comes to MHFP and MPFB electrolytes, the assembled Mg||Mg symmetric cells not only generate SEI after 5 cycles, but also stabilize after 10 cycles, and the Rs of cells show a negligible change (from 5.3 Ω to 8.3 Ω and 3.5 Ω to 6.8 Ω, respectively) as the cycle proceeds (Figure 3c and d). Corroborated with the fast Mg redox kinetics and high CEs, this in situ generated robust SEI can effectively protect Mg anode and enable good long-term cycling stability. Table S5 summarizes the fitted parameters of the in situ EIS for different electrolytes and the formation process of SEI is shown in Figure 3e.

Based on the EIS results, we can access the evolution mechanism of anode-electrolyte interface in fluoride alkyl electrolytes. However, the components of SEI are not clear enough, which motivates us to proceed X-ray photoelectron spectroscopy (XPS) and time-of-flight secondary-ion mass spectrometry (TOF-SIMS) to profile the SEI in depth. For Mg anode cycled in MPFB electrolyte, the C=O (532.5 eV) attributable to the solvent decomposition is observed before sputtering, and then the oxide peaks (529.9 eV) gradually dominate (Figure 4a).[32] It is worth mentioning that the cell disassembly and XPS samples preparation were carried out in an argon-filled glove box, so the interference of oxygen in the air can be excluded. Then, the Cl 2p XPS spectra (198.6 eV and 202.2 eV) were present throughout the sputtering process suggesting the vertical homogeneous distribution of chlorides (Figure 4e). In addition, SEI layers were also found to be rich in Mg^{2+} (50.4 eV) and Al^{3+} (74.1 eV) (Figure 4b and d), which reveals the uniform distribution of metal oxides and metal chlorides. However, the depth profiles of above elements exhibited ignorable discrepancies in cycled Mg anode from three fluoride alkyl electrolytes (Figure S16–S18), so we switched our attention to F element. The F 1s spectra reveal the presence of two distinct chemical states of F in SEI, where the signal at 688.4 eV should be assigned to the C–F bond in $–CF_3$ group and the signal at 685.3 eV should be attributed to MgF_2 (Figure 4c, Figure S16c, and Figure S17c).[33] After 60 s of sputtering, only the signal of MgF_2 can be detected, which may be attributed to the incomplete decomposition of the anion on the surface. Upon further sputtering, the F 1s XPS spectra show a remarkable difference, where the Mg anode cycled in MPFB electrolyte exhibits a significant MgF_2 signal, while the Mg anode cycled in the MHFP electrolyte shows a moderate MgF_2 signal, and the Mg anode cycled in MTFE electrolyte contains a weak MgF_2 signal. The intensity of MgF_2 in SEI layers is correlated linearly with the degree of fluorination of $Mg(OR^F)_2$ salts in the electrolyte. And MgF_2 can stabilize Mg anode due to its superior

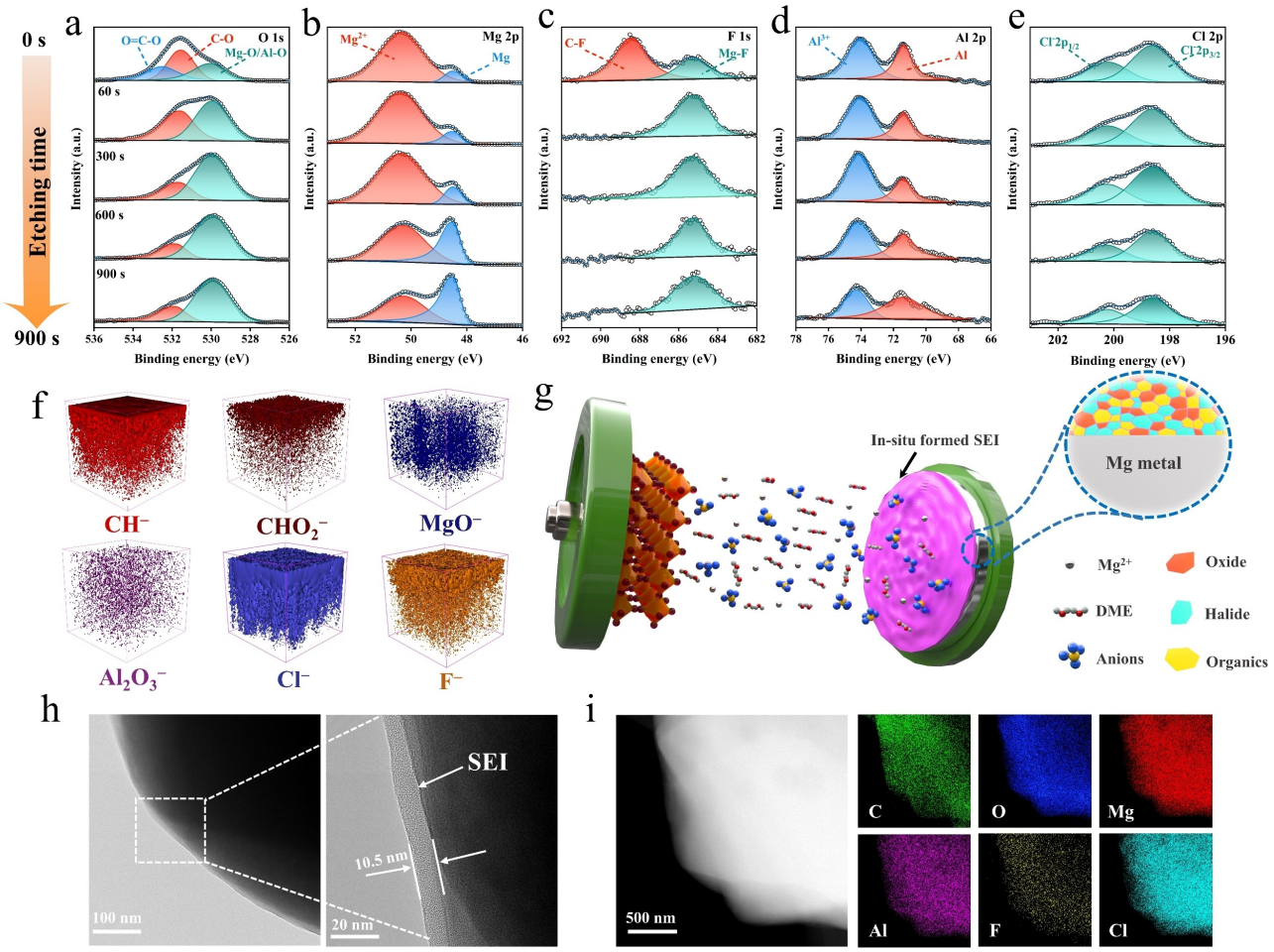

Figure 4. Constituents of the in situ generated SEI layer. XPS etching analysis of the Mg anode after cycling in MPFB electrolyte, a) O 1s, b) Mg 2p, c) F 1s, d) Al 2p, and e) Cl 2p. f) TOF-SIMS 3D rendering models of CH^-, CHO_2^-, MgO^-, $Al_2O_3^-$, Cl^-, and F^- for the cycled Mg anode in MPFB electrolyte. g) Schematic diagram of a Mg metal battery with in situ formed SEI. h) TEM images and an enlarged view at the cycles framed by the dashed rectangles. i) HAADF-STEM image and EDS elemental mappings of the in situ generated SEI layer in MPFB electrolyte.

mechanical and electrical insulating properties.[27c,34] Based on this, we concluded that the SEI generated from the MTFE electrolyte is fragile due to the low amount of MgF_2. In contrast, the MPFB electrolyte produces a vertically homogeneous MgF_2-rich SEI, which is responsible for stable Mg plating/stripping behavior. The TOF-SIMS results of cycled Mg anode in MPFB electrolyte also corroborate our conclusions, the CH^- and CHO_2^- enriched at the top of the SEI layer are derived from organic components, and the F^-, Cl^-, MgO^-, and $Al_2O_3^-$ signals are uniformly distributed (Figure 4f, Figure S19). Combining XPS and TOF-SIMS results, we can obtain the three-dimensional structure of this SEI (Figure 4g). Firstly, underlying it are uniformly distributed metal oxides and metal chlorides, while crucially MgF_2 acts as a skeleton to stabilize the whole steric structure, then, an organic layer derived from the decomposition of electrolyte is on the surface. Such an organic–inorganic hybridized SEI can effectively protect the Mg anode.[35]

Transmission electron microscopy (TEM) and corresponding energy dispersive spectroscopy (EDS) were employed to further unveil the fine structure and elemental composition of SEI layer. The TEM sample was prepared by scraping the surface of Mg anode cycled in MPFB electrolyte. As shown in Figure 4h, the compact nanoscale SEI can be clearly observed, and the even distribution of C, O, Mg, Al, F. The existence of Al elements confirms the SEI is formed from electrolyte decomposition (Figure 4i). Eventually, the SEI layer's thickness and impedance analysis revealed an ionic conductivity of $5.02\times10^{-8}\,S\,cm^{-1}$, which facilitating fast Mg^{2+} transport.[36]

Chevrel phase Mo_6S_8 cathode was used to evaluate the compatibility of fluoride alkyl electrolytes. The X-ray diffraction (XRD) pattern and morphology of the cathode material are shown in Figure S20 and Figure S21, respectively. The CV curves of Mg||Mo_6S_8 batteries using MACC and MTFE electrolytes only show a pair of redox peaks with larger polarization and lower intensity (Figure 5a), which is consistent with previous reports in literature. However, two pairs of redox peaks were observed in the CV curves of Mg||Mo_6S_8 batteries using MHFP and MPFB electrolytes, which might be associated with the influence of electrolyte composition on the intercalation process of Mg^{2+}, and more

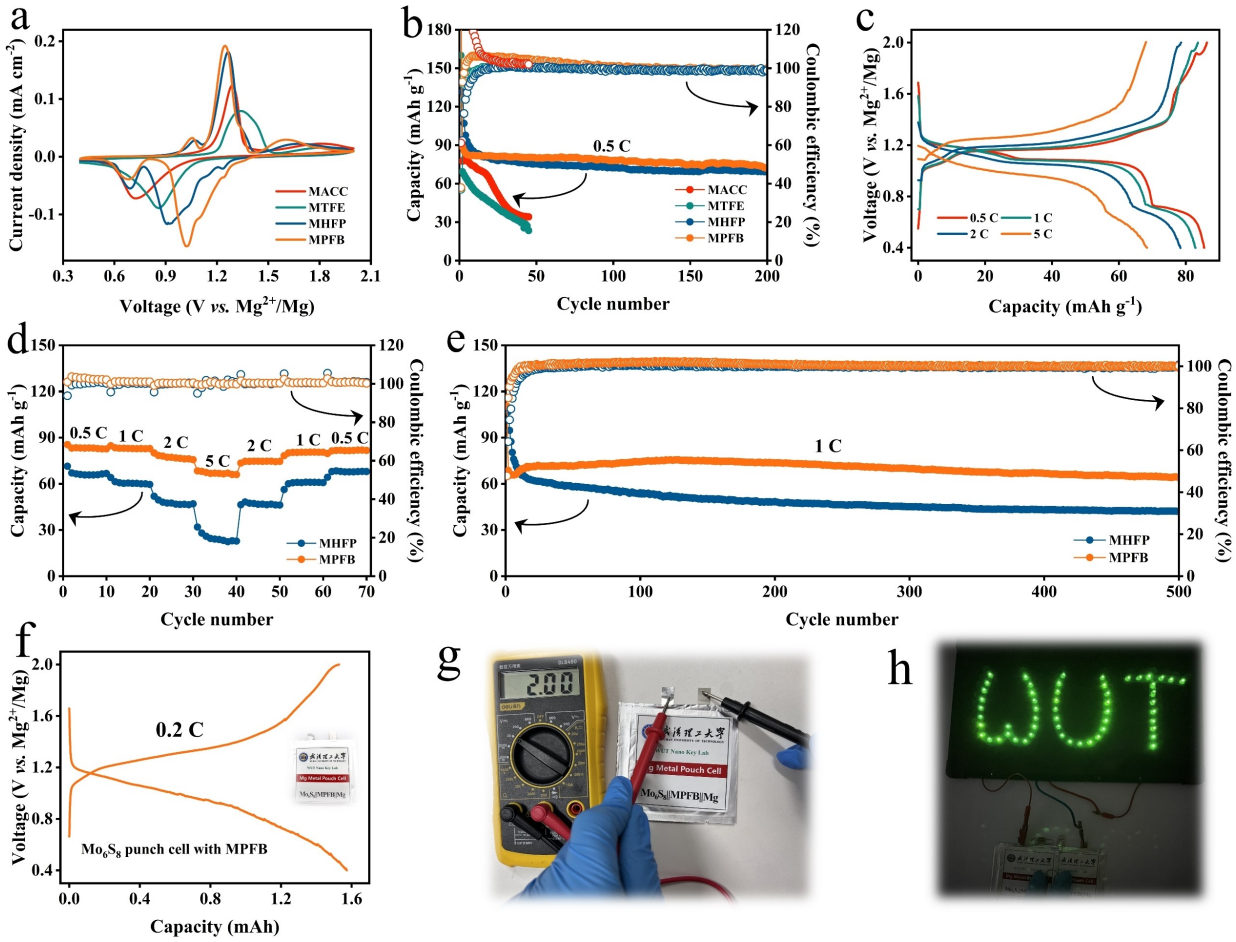

Figure 5. Mg||Mo_6S_8 full cell performance in different electrolyte. a) Cyclic voltammograms with a scan rate of 0.1 mV s^{-1}. b) Cycling performance over 200 cycles at 0.5 C (1 C = 128.8 mAh g^{-1}). c) Charge/discharge profile with a voltage range of 0.4–2.0 V (vs. Mg/Mg^{2+}) in MPFB electrolyte at various current densities. d) Rate performance at various current densities from 0.5 to 5 C. e) Long-term cycling performance at 1 C. f) Charge/discharge profile of Mg||Mo_6S_8 pouch cell with MPFB electrolyte at 0.2 C. g) Open circuit potential of the Mg||Mo_6S_8 pouch cell. h) The LEDs lightened by the Mg||Mo_6S_8 pouch cells in MPFB electrolytes.

Mg^{2+} storage sites were activated.[11] More importantly, the Mg||Mo_6S_8 battery using MPFB electrolyte with a more stable SEI demonstrates the minimum polarization voltage and maximum current intensity, suggesting that the robust anode-electrolyte interface is also critical for rapid Mg^{2+} interfacial transfer kinetics. The Mg||Mo_6S_8 full cells with different electrolytes also show significant discrepancies in cycling stability (Figure 5b). The Mg||Mo_6S_8 full cells using MACC and MTFE electrolytes exhibit rapid capacity decay during cycling and eventually failed, while the cells using MHFP and MPFB electrolytes deliver decent capacity (69.1 mAh g^{-1}, 72.1 mAh g^{-1}, respectively) as well as 99 % CEs after 200 cycles at 0.5 C. Moreover, the Mg||Mo_6S_8 full cell using MPFB electrolyte showed superior rate performance (Figure 5c and d). Specifically, the charge/discharge curves from 0.5 to 5 C show small changes in polarization, and a considerable capacity of 68.4 mAh g^{-1} is maintained at 5 C. In contrast, the Mg||Mo_6S_8 full cell using MHFP electrolyte displays low capacity of only 25.9 mAh g^{-1} at 5 C. In addition, the full cell with MPFB electrolyte delivers a high capacity retention of 93 % (64.4 mAh g^{-1}) after 500 cycles at 1 C compared with only 45 % (42.2 mAh g^{-1}) in MHFP electrolyte (Figure 5e). Further, the Mg||Mo_6S_8 pouch cells with MPFB electrolyte were assembled and successfully lit a light emitting diode (LED) board (Figure 5f–g), demonstrating the practical potential of this electrolyte.

Moreover, even in conventional sulfides (CuS) or high-voltage manganese oxides (Mg_xMnO_2) (Figure S22 and S23),[37] MPFB electrolyte also exhibits decent electrochemical performance and high oxidation stability (Figure S24 and S25), which reveals the good cathode-electrolyte compatibility. Besides, the SEI-protected Mg anode (after cycling in MPFB electrolyte) also behaved well in Mg-$(TFSI)_2$-based electrolytes (Figure S26), which confirmed the effectiveness of this SEI layer.

Conclusion

In summary, this work provides an insight view regarding the application of fluoride alkyl Mg salts in electrolytes.

Reconstructing the solvation structure of Mg^{2+} not only improves the high voltage tolerance of the electrolyte, but also contributes to the in situ formation of robust MgF_2-rich SEI. Among them, electrolytes configured with the most fluorinated $Mg(PFTB)_2$ can achieve a high oxidation stability of 4.0 V (vs. Mg/Mg^{2+}) and maintain ultra-high CE (99.5 %). These features also enable long-term Mg||Mg symmetric cell and $Mg||Mo_6S_8$ full cell cycle. Through stereoscopic, multi-view characterization of the SEI layer, we have also concluded that the uniform MgF_2 distribution contributes to the long-term stable cycling of the Mg anode. We believe that rational design and synthesis of Mg salts can empower the electrolyte field with more possibilities in the future.

Acknowledgements

This work was supported by the National Natural Science Foundation of China (51972259, 52172231, 52127816, 52202290, and 51832004), the National Key Research and Development Program of China (2020YFA0715000), the Natural Science Foundation of Hubei Province (2022CFA087), Industrialization Project of Xiangyang Technology Transfer Center of Wuhan University of Technology (WXCJ-20220017).

Conflict of Interest

The authors declare no conflict of interest.

Data Availability Statement

The data that support the findings of this study are available from the corresponding author upon reasonable request.

Keywords: Electrolyte · Fluoride Alkyl Magnesium Salts · Rechargeable Magnesium Batteries · Solid Electrolyte Interface

[1] a) Y. Liang, H. Dong, D. Aurbach, Y. Yao, *Nat. Energy* **2020**, *5*, 646–656; b) X. Liu, A. Du, Z. Guo, C. Wang, X. Zhou, J. Zhao, F. Sun, S. Dong, G. Cui, *Adv. Mater.* **2022**, *34*, 2201886; c) R. Davidson, A. Verma, D. Santos, F. Hao, C. Fincher, S. Xiang, J. Van Buskirk, K. Xie, M. Pharr, P. P. Mukherjee, S. Banerjee, *ACS Energy Lett.* **2019**, *4*, 375–376.

[2] a) S. Hou, X. Ji, K. Gaskell, P.-f. Wang, L. Wang, J. Xu, R. Sun, O. Borodin, C. Wang, *Science* **2021**, *374*, 172–178; b) Y. Zhu, X. Guo, Y. Lei, W. Wang, A.-H. Emwas, Y. Yuan, Y. He, H. N. Alshareef, *Energy Environ. Sci.* **2022**, *15*, 1282–1292; c) H. Dong, O. Tutusaus, Y. Liang, Y. Zhang, Z. Lebens-Higgins, W. Yang, R. Mohtadi, Y. Yao, *Nat. Energy* **2020**, *5*, 1043–1050.

[3] a) S. B. Son, T. Gao, S. P. Harvey, K. X. Steirer, A. Stokes, A. Norman, C. Wang, A. Cresce, K. Xu, C. Ban, *Nat. Chem.* **2018**, *10*, 532–539; b) Y. Zhao, A. Du, S. Dong, F. Jiang, Z. Guo, X. Ge, X. Qu, X. Zhou, G. Cui, *ACS Energy Lett.* **2021**, *6*, 2594–2601.

[4] a) R. Attias, M. Salama, B. Hirsch, Y. Goffer, D. Aurbach, *Joule* **2019**, *3*, 27–52; b) W. Zhao, Z. Pan, Y. Zhang, Y. Liu, H. Dou, Y. Shi, Z. Zuo, B. Zhang, J. Chen, X. Zhao, X. Yang, *Angew. Chem. Int. Ed.* **2022**, *61*, e202205187.

[5] D. Aurbach, Z. Lu, A. Schechter, Y. Gofer, H. Gizbar, R. Turgeman, Y. Cohen, M. Moshkovich, E. Levi, *Nature* **2000**, *407*, 724–727.

[6] O. Mizrahi, N. Amir, E. Pollak, O. Chusid, V. Marks, H. Gottlieb, L. Larush, E. Zinigrad, D. Aurbach, *J. Electrochem. Soc.* **2008**, *155*, A103.

[7] F. F. Wang, Y. S. Guo, J. Yang, Y. Nuli, S. Hirano, *Chem. Commun.* **2012**, *48*, 10763–10765.

[8] a) R. E. Doe, R. Han, J. Hwang, A. J. Gmitter, I. Shterenberg, H. D. Yoo, N. Pour, D. Aurbach, *Chem. Commun.* **2014**, *50*, 243–245; b) J. Luo, S. He, T. L. Liu, *ACS Energy Lett.* **2017**, *2*, 1197–1202.

[9] a) H. Zhang, L. Qiao, M. Armand, *Angew. Chem. Int. Ed.* **2022**, *61*, e202214054; b) J. Muldoon, C. B. Bucur, T. Gregory, *Angew. Chem. Int. Ed.* **2017**, *56*, 12064–12084; c) N. T. Hahn, T. J. Seguin, K. C. Lau, C. Liao, B. J. Ingram, K. A. Persson, K. R. Zavadil, *J. Am. Chem. Soc.* **2018**, *140*, 11076–11084.

[10] a) Z. Zhao-Karger, R. Liu, W. Dai, Z. Li, T. Diemant, B. P. Vinayan, C. Bonatto Minella, X. Yu, A. Manthiram, R. J. Behm, M. Ruben, M. Fichtner, *ACS Energy Lett.* **2018**, *3*, 2005–2013; b) P. Jankowski, Z. Li, Z. Zhao-Karger, T. Diemant, M. Fichtner, T. Vegge, J. M. G. Lastra, *Energy Storage Mater.* **2022**, *45*, 1133–1143.

[11] W. Ren, D. Wu, Y. NuLi, D. Zhang, Y. Yang, Y. Wang, J. Yang, J. Wang, *ACS Energy Lett.* **2021**, *6*, 3212–3220.

[12] a) J. Luo, Y. Bi, L. Zhang, X. Zhang, T. L. Liu, *Angew. Chem. Int. Ed.* **2019**, *58*, 6967–6971; b) O. Tutusaus, R. Mohtadi, T. S. Arthur, F. Mizuno, E. G. Nelson, Y. V. Sevryugina, *Angew. Chem. Int. Ed.* **2015**, *54*, 7900–7904.

[13] J. Xiao, X. Zhang, H. Fan, Y. Zhao, Y. Su, H. Liu, X. Li, Y. Su, H. Yuan, T. Pan, Q. Lin, L. Pan, Y. Zhang, *Adv. Mater.* **2022**, *34*, 2203783.

[14] J. T. Herb, C. A. Nist-Lund, C. B. Arnold, *ACS Energy Lett.* **2016**, *1*, 1227–1232.

[15] D. Huang, S. Tan, M. Li, D. Wang, C. Han, Q. An, L. Mai, *ACS Appl. Mater. Interfaces* **2020**, *12*, 17474–17480.

[16] a) Y. Yang, W. Wang, Y. Nuli, J. Yang, J. Wang, *ACS Appl. Mater. Interfaces* **2019**, *11*, 9062–9072; b) M. Ulaganathan, C. M. Mathew, S. Rajendran, *Electrochim. Acta* **2013**, *93*, 230–235.

[17] M. Cheng, W. Ren, D. Zhang, S. Zhang, Y. Yang, X. Lv, J. Yang, J. Wang, Y. NuLi, *Energy Storage Mater.* **2022**, *51*, 764–776.

[18] A. Du, Z. Zhang, H. Qu, Z. Cui, L. Qiao, L. Wang, J. Chai, T. Lu, S. Dong, T. Dong, H. Xu, X. Zhou, G. Cui, *Energy Environ. Sci.* **2017**, *10*, 2616–2625.

[19] a) Z. Zhao-Karger, X. Zhao, D. Wang, T. Diemant, R. J. Behm, M. Fichtner, *Adv. Energy Mater.* **2015**, *5*, 1401155; b) Z. Zhang, Z. Cui, L. Qiao, J. Guan, H. Xu, X. Wang, P. Hu, H. Du, S. Li, X. Zhou, S. Dong, Z. Liu, G. Cui, L. Chen, *Adv. Energy Mater.* **2017**, *7*, 1602055.

[20] Y. Li, S. Guan, H. Huo, Y. Ma, Y. Gao, P. Zuo, G. Yin, *Adv. Funct. Mater.* **2021**, *31*, 2100650.

[21] T. Lu, F. Chen, *J. Comput. Chem.* **2012**, *33*, 580–592.

[22] J. Holoubek, Q. Yan, H. Liu, E. J. Hopkins, Z. Wu, S. Yu, J. Luo, T. A. Pascal, Z. Chen, P. Liu, *ACS Energy Lett.* **2022**, *7*, 675–682.

[23] a) N. Yao, S.-Y. Sun, X. Chen, X.-Q. Zhang, X. Shen, Z.-H. Fu, R. Zhang, Q. Zhang, *Angew. Chem. Int. Ed.* **2022**, *61*, e202210859; b) X. Chen, X. Shen, T.-Z. Hou, R. Zhang, H.-J. Peng, Q. Zhang, *Chem* **2020**, *6*, 2242–2256.

[24] Y.-s. Guo, F. Zhang, J. Yang, F.-f. Wang, Y. NuLi, S.-i. Hirano, *Energy Environ. Sci.* **2012**, *5*, 9100–9106.

[25] Y. Zhao, T. Zhou, T. Ashirov, M. E. Kazzi, C. Cancellieri, L. P. H. Jeurgens, J. W. Choi, A. Coskun, *Nat. Commun.* **2022**, *13*, 2575.
[26] S. Zhang, M. Cheng, P. Zhang, Y. Wang, D. Zhang, Y. Yang, J. Wang, Y. NuLi, *Chem. Commun.* **2022**, *58*, 11969–11972.
[27] a) J. Zhang, X. Guan, R. Lv, D. Wang, P. Liu, J. Luo, *Energy Storage Mater.* **2020**, *26*, 408–413; b) H. Fan, Z. Zheng, L. Zhao, W. Li, J. Wang, M. Dai, Y. Zhao, J. Xiao, G. Wang, X. Ding, H. Xiao, J. Li, Y. Wu, Y. Zhang, *Adv. Funct. Mater.* **2020**, *30*, 1909370; c) K. Tang, A. Du, S. Dong, Z. Cui, X. Liu, C. Lu, J. Zhao, X. Zhou, G. Cui, *Adv. Mater.* **2020**, *32*, 1904987; d) G. Yang, Y. Li, C. Zhang, J. Wang, Y. Bai, C. Y. J. Lim, M.-F. Ng, Z. Chang, S. Kumar, Z. Sofer, W. Liu, Z. W. Seh, *Nano Lett.* **2022**, *22*, 9138–9146; e) R. Horia, D.-T. Nguyen, A. Y. S. Eng, Z. W. Seh, *Nano Lett.* **2021**, *21*, 8220–8228; f) W. Li, S. Cheng, J. Wang, Y. Qiu, Z. Zheng, H. Lin, S. Nanda, Q. Ma, Y. Xu, F. Ye, M. Liu, L. Zhou, Y. Zhang, *Angew. Chem. Int. Ed.* **2016**, *55*, 6406–6410.
[28] Z. Liang, C. Ban, *Angew. Chem. Int. Ed.* **2021**, *60*, 11036–11047.
[29] D. Han, C. Cui, K. Zhang, Z. Wang, J. Gao, Y. Guo, Z. Zhang, S. Wu, L. Yin, Z. Weng, F. Kang, Q.-H. Yang, *Nat. Sustainability* **2022**, *5*, 205–213.
[30] B. Roy, P. Cherepanov, C. Nguyen, C. Forsyth, U. Pal, T. C. Mendes, P. Howlett, M. Forsyth, D. MacFarlane, M. Kar, *Adv. Energy Mater.* **2021**, *11*, 2101422.
[31] H. Dou, X. Zhao, Y. Zhang, W. Zhao, Y. Yan, Z.-F. Ma, X. Wang, X. Yang, *Nano Energy* **2021**, *86*, 106087.
[32] J. Xiao, X. Zhang, H. Fan, Q. Lin, L. Pan, H. Liu, Y. Su, X. Li, Y. Su, S. Ren, Y. Lin, Y. Zhang, *Adv. Energy Mater.* **2022**, *12*, 2202602.
[33] Z. Yu, P. E. Rudnicki, Z. Zhang, Z. Huang, H. Celik, S. T. Oyakhire, Y. Chen, X. Kong, S. C. Kim, X. Xiao, H. Wang, Y. Zheng, G. A. Kamat, M. S. Kim, S. F. Bent, J. Qin, Y. Cui, Z. Bao, *Nat. Energy* **2022**, *7*, 94–106.
[34] B. Li, R. Masse, C. Liu, Y. Hu, W. Li, G. Zhang, G. Cao, *Energy Storage Mater.* **2019**, *22*, 96–104.
[35] Y. Y. Hwang, N. K. Lee, S. H. Park, J. Shin, Y. J. Lee, *Energy Storage Mater.* **2022**, *51*, 108–121.
[36] Y. Zhang, J. Li, W. Zhao, H. Dou, X. Zhao, Y. Liu, B. Zhang, X. Yang, *Adv. Mater.* **2022**, *34*, 2108114.
[37] Z. Yang, X. Pan, Y. Shen, R. Chen, T. Li, L. Xu, L. Mai, *Small* **2022**, *18*, 2107743.

Manuscript received: February 7, 2023
Accepted manuscript online: March 22, 2023
Version of record online: ■■, ■■

Research Articles

Mg Metal Batteries

J. Long, S. Tan, J. Wang, F. Xiong, L. Cui, Q. An,* L. Mai* ——— e202301934

Revealing the Interfacial Chemistry of Fluoride Alkyl Magnesium Salts in Magnesium Metal Batteries

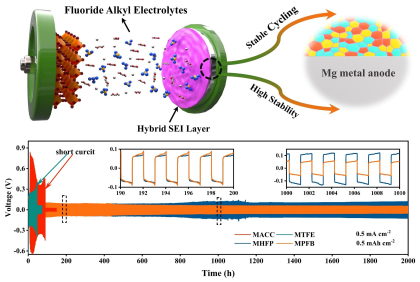

Fluoride alkyl magnesium salts reconstructing the solvation structure of Mg^{2+} not only improves the high voltage tolerance of the electrolyte, but also facilitates in situ generation robust solid electrolyte interface enabling steady Mg metal anode.